

phase, presenting evidence of correlations at extended distances that we have measured using the mutual information metric.

This paper continues as follows. In Sec. II, the computational procedure is described in detail. Sec. III presents the main simulation and statistical results, while the paper concludes in Sec. IV with some final remarks.

II. COMPUTATIONAL PROCEDURE

In this work we performed a number of microcanonical (NVE) MD simulations at different initial temperatures T_0 , equivalent to different total energies of the system through the relation

$$E = \frac{3}{2} N k_B T_0 + \Phi_0,$$

with Φ_0 the potential energy of the ideal crystal. In our case, $\Phi_0 = 556.74$ eV. We considered as a starting point for these MD simulations a perfect crystal of argon, corresponding to a face-centered-cubic (FCC) structure, and interacting through a standard Lennard-Jones (LJ) potential,

$$\begin{aligned} \Phi(\mathbf{r}_1, \dots, \mathbf{r}_N) &= \sum_i \Phi_i(\mathbf{r}_1, \dots, \mathbf{r}_N) \\ &= \sum_i \left[\frac{1}{2} \sum_{j \neq i} \varphi(|\mathbf{r}_i - \mathbf{r}_j|) \right], \end{aligned} \quad (1)$$

where $\varphi(r)$ is the pair potential function,

$$\varphi(r) = 4\epsilon \left[\left(\frac{\sigma}{r} \right)^{12} - \left(\frac{\sigma}{r} \right)^6 \right].$$

The crystal is simulated at high density in order to enhance the superheating effect, using a lattice constant $a = 4.2$ Å and the usual LJ parameters for argon, namely $\epsilon/k_B = 119.8$ K and $\sigma = 3.41$ Å. All MD simulations were performed using the LPMO package [29], with a timestep $\Delta t = 1$ fs. For every value of initial temperature T_0 we used a total simulation time of 80 ps, corresponding to 80000 steps.

As shown in Fig.1, through the use of the Z-method we have obtained an isochoric curve with a melting temperature $T_m = 5231$ K and superheating temperature $T_{LS} = 6695$ K. Also a critical energy $E_{LS} = 1976$ eV was obtained, such that it is impossible to administer additional energy without the system melting spontaneously.

The regions of thermodynamic stability are given by $E < 1600$ eV ($T < T_m$), where the solid phase is stable, and $E > 1976$ eV where the liquid phase becomes stable. For energies between 1600 eV and 1850 eV the system is found in a metastable, superheated solid phase, while in the region between $E=1850$ eV and $E=2050$ eV, the system exists in either of two phases, namely superheated solid or liquid.

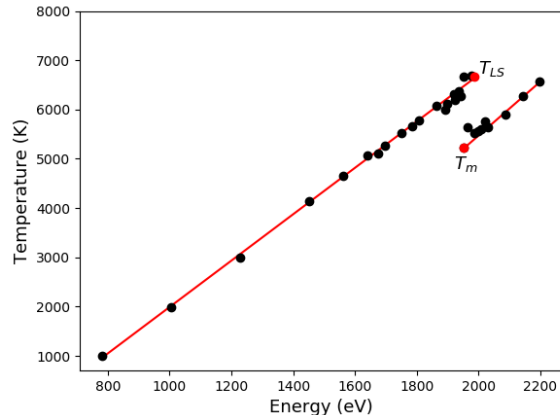


FIG. 1. Isochoric (Z) curve obtained from 31 different 80 ps simulations of high-density Ar, with initial temperatures T_0 ranging from 2000 to 12600 K. From this Z-curve we can determine $T_m \sim 5231$ K and $T_{LS} \sim 6695$ K.

In the next section we present the results obtained from MD simulation, which we have used to establish the probability distribution describing the potential energy per atom ϕ as a function of total energy E . Moreover, we present evidence for the existence of increasing correlation between atoms at long-range distances as the temperature increases, as measured through the mutual information metric.

III. RESULTS

Fig. 2 shows a typical microcanonical simulation during which melting is triggered spontaneously. The instantaneous temperature of the system, originally prepared at $T_0 = 12600$ K from an ideal crystalline structure, first drops to approximately 6500 K due to the equilibration of potential and kinetic energies. At this point the system remains in a metastable, superheated solid state. After $t_w=9$ ps for this particular simulation, the crystal suddenly collapses and the temperature drops to about 5500 K. For several simulations at the same total energy we obtained random melting times ranging from 1 to 80 ps, which is consistent with previous studies of the kinetics of homogeneous melting [30, 31]. In terms of the atomistic dynamics, the picture is as follows. As the system begins to evolve from the ideal crystalline structure, the atoms begin to move away from their stable local potential energy minima. For temperatures above T_m the energy per atom is such that thermally-activated point defects start to form [32]. This increase of the number of defects and their mobility results in a cooperative motion involving several atoms.

In order to reveal the existence of extreme events and interatomic correlations in the superheated phase, we

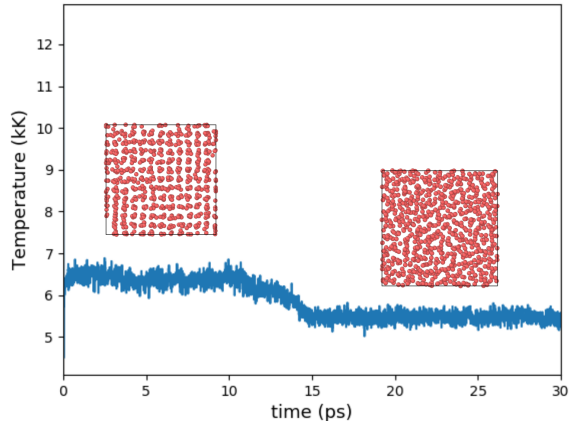


FIG. 2. Instantaneous temperature $T(t)$ for a simulation at an initial temperature $T_0 = 12600$ K. Only the first 30 ps of the simulation are shown, as after the melting process occurs at time $t_w = 9$ ps the system remains in the liquid phase.

have studied the statistics of the potential energy per atom ϕ . In the low-temperature, harmonic approximation of a solid, each atom moves independently as an harmonic oscillator anchored to its equilibrium position. It can be shown that for the microcanonical ensemble in the limit $N \rightarrow \infty$ (see the Appendix for more details), the probability distribution function of ϕ for non-interacting particles is given by

$$P(\phi_i|E) = \frac{1}{Z_1(\beta)} \exp(-\beta\phi_i) \Omega_1(\phi_i), \quad (2)$$

with $\beta = 3N/2E$. In the superheated solid, however, we have found that ϕ follows a gamma distribution,

$$P(\phi|E) = P(\phi|k, \theta) = \frac{\exp(-\phi/\theta)\phi^{k-1}}{\Gamma(k)\theta^k}, \quad (3)$$

with energy-dependent parameters $k = k(E)$ and $\theta = \theta(E)$. Fig. 3 shows an example of this distribution for $T_0 = 10000$ K, having a most probable energy given by the mode of the gamma distribution, $\phi^* = (k-1)\theta$, in this case corresponding to $\phi^* = 2.217$ eV.

Fig. 4 shows the probability density function $P(\phi|E)$ for different initial temperatures ranging from $T_0 = 2000$ K up to $T_0 = 12500$ K. Here we see that the observed $P(\phi|E)$ is incompatible with Eq. 2 for independent oscillators, because k depends on the total energy, and it is in fact described by

$$P(\phi_1|E) = \frac{1}{Z(\beta)} \exp(-\beta\phi_1) \omega_1(\phi_1; E) \quad (4)$$

as shown in the Appendix. Therefore, we can conclude at this point that the potential energies of different atoms are correlated up to some distance to be determined.

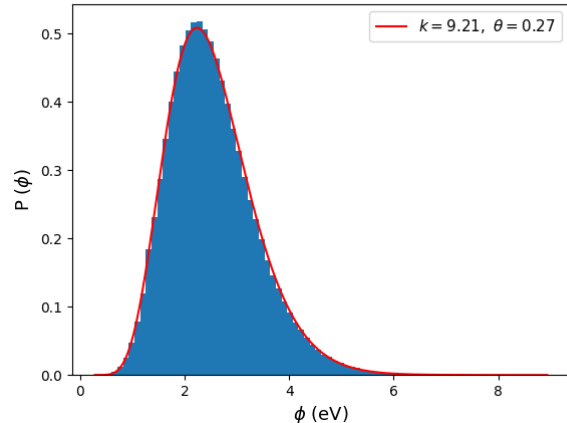


FIG. 3. Histogram of potential energy per atom for a system at $T_0 = 10000$ K (blue filled region) and gamma statistical distribution with parameters $k=9.21$ and $\theta=0.27$ eV (red curve).

While at low temperatures the potential energy values are in fact distributed following a Gaussian distribution, clearly indicating independent behavior compatible with Eq. 2, as the temperature of the system increases the atoms in the lattice break their symmetry. In this phase the solid is in superheated phase, producing a correlation of potential energies between nearest neighbors and even larger distances; these results are consistent with Eqs. 4 and 3. Note that in no case we observe a bimodal distribution of potential energies, as might be expected in the case of nucleation of a liquid phase inside a solid matrix.

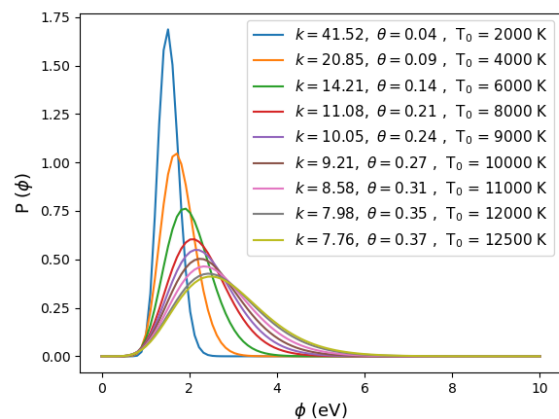


FIG. 4. Probability density function of single-atom potential energies $P(\phi|E)$ for different initial temperatures T_0 between 2000 K and 12500 K. The nearly Gaussian distribution for $T_0 = 2000$ K changes to a long-tailed distribution indicating correlations as the temperature T_0 increases.

In Figs. 5, 6 and 7 an energy of superheating between 1640 and 1936 eV can be observed. It is important to notice that the parameters k and θ present a dependence on the total energy of the system. From a total energy $E = 1947$ eV upwards, the system is present in one of two possible phases: critical superheated solid and liquid. Here we can see two branches where the parameters k and θ are found in the same phase of the superheated solid. The variation of these parameters with the total energy is an important indicator of the existence of correlations between atoms, where possibly every atom depends on the behavior of its nearest neighbors and even beyond third-nearest neighbors.

Fig. 5 shows the behavior of the shape parameter k as a function of the total energy E . As the system does not behave like a collection of independent harmonic oscillators, but is correlated, the *effective* degrees of freedom are now determined by the “density of states” factor in Eq. 3, governed by the exponent $k(E)$. As seen in the figure, for higher energies k decreases, hence a reduced number of configurations are available for each atom at a given potential energy ϕ which again is suggestive of a cooperative motion.

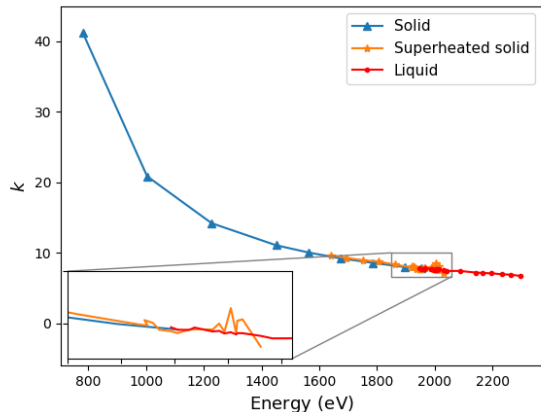


FIG. 5. Shape parameter k as a function of the energy E . The solid, light blue line represents the system in its solid phase, the yellow line in its superheated solid phase and the red line in liquid phase. From the energy $E=1947$ eV to $E=2031$ eV, the system is in the critical superheated phase.

On the other hand, Fig. 6 shows that the scale parameter θ does not present a continuous behavior as a function of energy. The discontinuity is essentially due to the latent heat per atom, which corresponds to the change in potential energy as the system undergoes the phase transition.

Fig. 7 shows the expected value of potential energy per atom as a function of the total energy E , that is, $\langle \phi \rangle_E$, which is given by $k\theta$ in terms of the Gamma parameters. We can clearly see that $\langle \phi \rangle_E$ increases linearly with E in both the solid and liquid branches (outside the

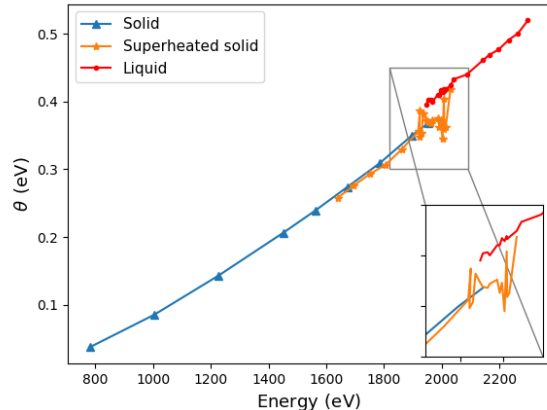


FIG. 6. Scale parameter θ as a function of the energy E . The solid, light blue line represents the system in its solid phase, the yellow line in its superheated solid phase and the red line in liquid phase. From the energy $E=1947$ eV to $E=2031$ eV the system is in the critical superheated phase.

metastable region), as expected in a system with constant specific heat in their stable phases.

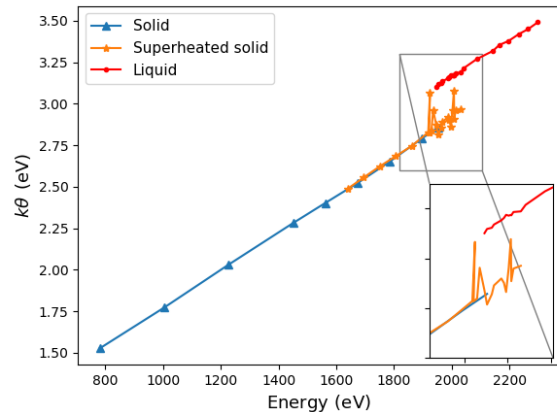


FIG. 7. Expected value $\langle \phi \rangle_E = k\theta$ as a function of energy E . The solid, light blue line represents the system in its solid phase, the yellow line in its superheated solid phase and the red line in liquid phase. From the energy $E=1947$ eV to $E=2031$ eV the system is in critical superheated phase.

From Eq. 14 for $P(\phi_1, \phi_2|E)$ we performed a non-parametric estimation of the joint distribution using the kernel density estimation (KDE) method [33], considering data from the MD simulations where a set of potential energies ϕ_1, \dots, ϕ_N are divided into pairs at given distances r . This kernel density estimation is shown in Figs. 8 and 9 for a dataset of potential energies at initial temperatures $T_0=2000$ K and $T_0=12500$ K, respectively at a distance of $r = 7.25$ Å. For $T_0 = 2000$ K, the po-

tential energy pairs follow a bivariate Gaussian [33] with almost null correlation. However, for $T_0 = 12500$ K a kind of directionality in the shape of the bidimensional distribution can be seen, in a consistent manner with the marginal Gamma distributions, which confirms the presence of correlations between distant pairs of atoms at high temperatures.

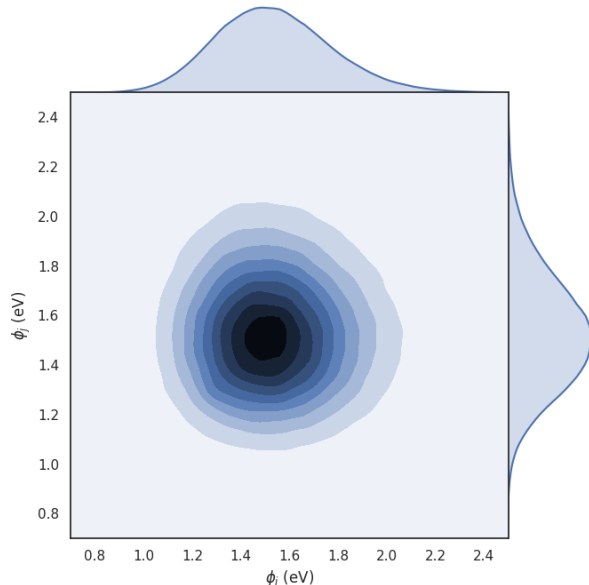


FIG. 8. Kernel density estimation of the joint distribution $P(\phi_1, \phi_2 | E)$ for a distance $r = 7.25$ Å and initial temperature $T_0 = 2000$ K. At low temperature the system does not present a correlation, distributing the potential energies by means of a Gaussian distribution in 2D.

As an indicator of correlation between potential energies of distant atoms, we have computed the mutual information [22], which measures statistical dependence between two arbitrary random variables x and y , and is defined by

$$I = \int dx dy P(x, y | K) \ln \left[\frac{P(x, y | K)}{P(x | K)P(y | K)} \right], \quad (5)$$

where $P(x, y | K)$ is the joint probability distribution of x and y , and $P(x | K)$, $P(y | K)$ are the marginal probability distributions. The mutual information I is non-negative, and strictly zero only for statistically independent variables, as in this case $P(x, y | K) = P(x | K)P(y | K)$.

Fig. 10 shows the correlation, as measured by the mutual information diagnostic, between potential energies ϕ_1 and ϕ_2 of a pair of atoms as a function of their distance r . It can be seen that for low temperatures, around $T_0 = 2000$ K, the system presents only correlations for short distances, where the peaks are simply indicative of the direct interaction of the atoms with their immediate neighbor shells. However, at larger distances this correlation decays quickly, being almost

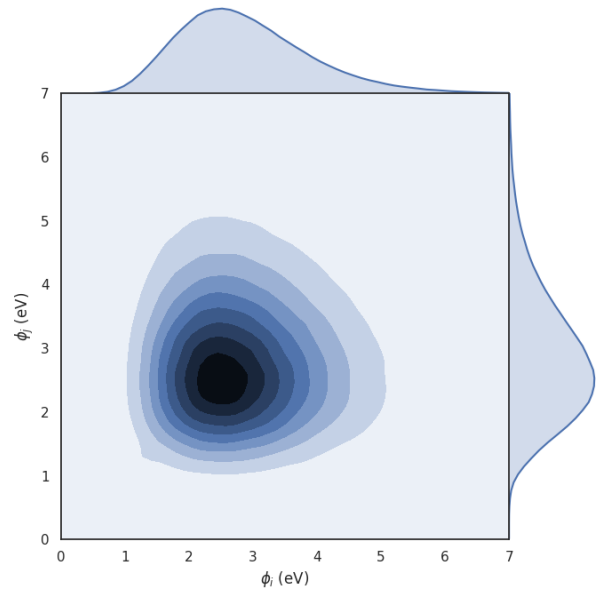


FIG. 9. Kernel density estimation of the joint distribution $P(\phi_1, \phi_2 | E)$ for a distance $r = 7.25$ Å and initial temperature $T_0 = 12500$ K. At high temperatures the system presents a correlation the potential energies are distributed according to a Gamma distribution.

zero beyond $r = 7.75$ Å. As the temperature is increased, the system gains energy and becomes metastable once it crosses T_m , with a clear increase in correlation. In Fig. 11 the mutual information $I(r; T_0)$ is shown as a function of the initial temperature T_0 at a fixed distance of $r = 7.25$ Å. Interestingly, we can see that the mutual information seems to exhibit a marked, almost linear dependence on T_0 which saturates close to T_{LS} .

At this point we have given a characterization of the superheated solid state in terms of some of its statistical properties. The emerging picture is one of increasing correlation between distant atoms and reduced configurational degrees of freedom per atom as the system approaches T_{LS} from below. In addition, note that it is possible to establish similarities with the glassy state (supercooled liquid), a metastable state occurring at temperatures lower than the melting temperature. In both cases the system is located in points outside the equilibrium phase, “locked” in a dynamical state that does not allow it to transition into the “correct” thermodynamical phase, and presenting nontrivial atomic kinetics.

Despite the fact that the case of superheated solid could seem opposite to the glassy state, apparently these transitions occur in a similar way, both involving cooperativity between their atoms, as the movement of one atom depends on the movement of the others. In both cases there is the presence of spatial correlations near the phase transition, in our case near the melting point. This cooperative movement implies a reduction of the effective

degrees of freedom, as shown in Figs. 5 and 11. As the energy increases, correlations increase at large distances between the potential energies of the atoms, as shown in Fig. 11, while in turn the number of effective degrees of freedom is reduced, as can be seen in Fig. 5, because these correlations limit the amount of allowed movements of the atoms.

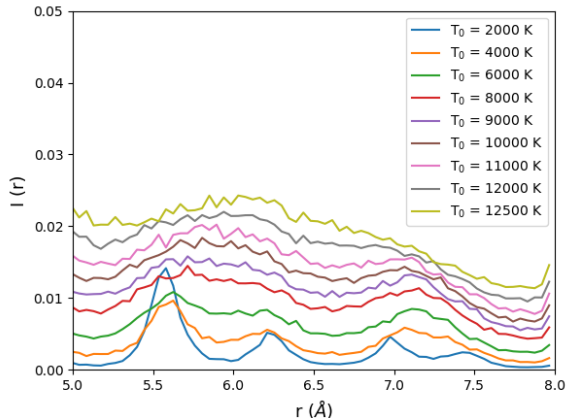


FIG. 10. Mutual information $I(r)$, as given in Eq. 5, as a function of the interatomic distance r . At long-range the correlation measured by $I(r)$ increases as the solid becomes metastable.

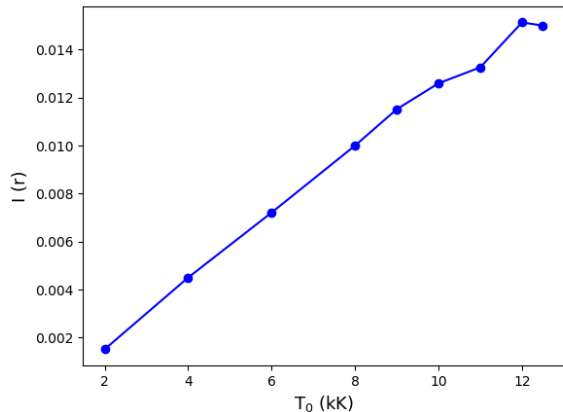


FIG. 11. Mutual information $I(r; T_0)$ as a function of the initial temperature T_0 at a fixed distance $r = 7.25$ Å. The values of $I(r; T_0)$ increase proportionally with the initial temperature, presenting a slight drop close to 12500 K.

IV. CONCLUDING REMARKS

Using microcanonical molecular dynamics simulations we have characterized the statistics of single-atom poten-

tial energies in the metastable solid prior to melting, according to a gamma distribution with energy-dependent parameters k and θ , which is consistent with correlated behavior. Furthermore, we have presented strong evidence confirming the emergence of long-range spatial correlations of potential energy in the critical superheated solid. These correlations may arise due to the cooperative dynamical processes occurring in the crystal after the creation of mobile vacancy-interstitial pairs.

ACKNOWLEDGEMENTS

This work is supported by FONDECYT grant 1171127 and Anillo ACT-172101. Computations were performed using the supercomputing infrastructure of FENIX, Materials Science Group, UNAB Physics Department (<http://www.matbio.cl/fenix>).

APPENDIX: MICROCANONICAL DISTRIBUTIONS OF POTENTIAL ENERGY

In the microcanonical ensemble, the probability density of microstates is given by

$$P(\mathbf{R}, \mathbf{P}|E) = \frac{\delta\left(E - \sum_i \frac{p_i^2}{2m_i} - \Phi(\mathbf{R})\right)}{\Omega(E)}, \quad (6)$$

with $\mathbf{R} = (\mathbf{r}_1, \dots, \mathbf{r}_N)$, $\mathbf{P} = (\mathbf{p}_1, \dots, \mathbf{p}_N)$ and where $\Omega(E)$ the density of states. By integration over \mathbf{P} it can be shown [34–36] that

$$P(\mathbf{r}_1, \dots, \mathbf{r}_N|E) = \frac{1}{\eta(E)} [E - \Phi(\mathbf{r}_1, \dots, \mathbf{r}_N)]_+^{\frac{3N}{2}-1}, \quad (7)$$

which in the limit $N \rightarrow \infty$ reduces to a canonical distribution,

$$P(\mathbf{r}_1, \dots, \mathbf{r}_N|E) = \frac{1}{Z(\beta)} \exp(-\beta\Phi(\mathbf{r}_1, \dots, \mathbf{r}_N)), \quad (8)$$

with $\beta = 3N/2E$. Therefore, the probability of observing a set of potential energies $\Phi_1 = \phi_1, \Phi_2 = \phi_2, \dots, \Phi_N = \phi_N$ at total energy E is given by

$$P(\phi_1, \dots, \phi_N|E) = \frac{1}{Z(\beta)} \exp\left(-\beta \sum_{i=1}^N \phi_i\right) \times \Omega_N(\phi_1, \dots, \phi_N), \quad (9)$$

where

$$\Omega_N(\phi_1, \dots, \phi_N) = \int d\mathbf{r}_1 \dots d\mathbf{r}_N \prod_{i=1}^N \delta(\Phi_i - \phi_i)$$

is the joint configurational density of states. For non-interacting atoms we have that $\Phi_i = \Phi_i(\mathbf{r}_i)$ and therefore

$$\begin{aligned}\Omega_N(\phi_1, \dots, \phi_N) &= \prod_{i=1}^N \left\{ \int d\mathbf{r} \delta(\Phi_i(\mathbf{r}) - \phi_i) \right\} \\ &= \prod_{i=1}^N \Omega_1(\phi_i),\end{aligned}\quad (10)$$

hence $P(\phi_1, \dots, \phi_N|E)$ factorizes and ϕ_i itself follows a canonical distribution

$$P(\phi_i|E) = \frac{1}{Z_1(\beta)} \exp(-\beta\phi_i) \Omega_1(\phi_i). \quad (11)$$

Here $\Omega_1(\phi) = \int d\mathbf{r} \delta(\phi - \Phi_1(\mathbf{r}))$ plays the role of a “density of states” factor which is independent of the total energy E . On the other hand, for interacting atoms the probability density $P(\phi_1|E)$ will be given by the marginalization of Eq. 9,

$$P(\phi_1|E) = \frac{1}{Z(\beta)} \exp(-\beta\phi_1) \omega_1(\phi_1; E) \quad (12)$$

where

$$\begin{aligned}\omega_1(\phi_1; E) &= \int d\phi_2 \dots d\phi_N \exp\left(-\frac{3N}{2E} \sum_{i=2}^N \phi_i\right) \\ &\quad \times \Omega_N(\phi_1, \dots, \phi_N).\end{aligned}\quad (13)$$

Now the “density of states” factor ω_1 is energy-dependent. Similarly, for the joint distribution $P(\phi_1, \phi_2|E)$ we obtain by marginalization

$$P(\phi_1, \phi_2|E) = \frac{\exp\left(-\frac{3N}{2E}(\phi_1 + \phi_2)\right)}{Z\left(\frac{3N}{2E}\right)} \times \omega_2(\phi_1, \phi_2; E), \quad (14)$$

where $\omega_2(\phi_1, \phi_2; E)$ is defined by

$$\begin{aligned}\omega_2(\phi_1, \phi_2; E) &= \int d\phi_3 \dots d\phi_N \exp\left(-\frac{3N}{2E} \sum_{i=3}^N \phi_i\right) \\ &\quad \times \Omega_N(\phi_1, \dots, \phi_N).\end{aligned}\quad (15)$$

-
- [1] Z. H. Jin, P. Gumbsch, K. Lu, and E. Ma, Phys. Rev. Lett. **87**, 055703 (2001).
- [2] S.-N. Luo and T. J. Ahrens, Appl. Phys. Lett. **82**, 1836 (2003).
- [3] M. Forsblom and G. Grimvall, Nature Materials **4**, 388 (2005).
- [4] X.-M. Bai and M. Li, J. Chem. Phys. **122**, 224510 (2005).
- [5] S.-N. Luo, L. Zheng, A. Strachan, and D. C. Swift, J. Chem. Phys. **126**, 034505 (2007).
- [6] A. B. Belonoshko, S. Davis, N. V. Skorodumova, P. H. Lundow, A. Rosengren, and B. Johansson, Phys. Rev. B **76**, 064121 (2007).
- [7] X.-M. Bai and M. Li, Phys. Rev. B **77**, 134109 (2008).
- [8] S. Davis, A. B. Belonoshko, B. Johansson, and A. Rosengren, Phys. Rev. B **84**, 064102 (2011).
- [9] L. C. Gallington and A. Bongiorno, J. Chem. Phys. **132**, 174707 (2010).
- [10] K. Binder and H. Müller-Krumbhaar, Phys. Rev. B **9**, 2328 (1974).
- [11] H. Tomita and S. Miyashita, Phys. Rev. B **46**, 8886 (1992).
- [12] F. Moreno, S. Davis, C. Loyola, and J. Peralta, Phys. A **509**, 361 (2018).
- [13] J. J. Wu, H. J. Sun, and Z. Y. Gao, Phys. Rev. E **78**, 036103 (2008).
- [14] R. Monasson, Physical Review Letters **75**, 2847 (1995).
- [15] A. Pluchino, V. Latora, and A. Rapisarda, Phys. D **193**, 315 (2004).
- [16] B. Doliwa and A. Heuer, Phys. Rev. E **61**, 6898 (2000).
- [17] A. S. Bakai, J. Non-Cryst. Solids **307**, 623 (2002).
- [18] A. S. Bakai and E. W. Fischer, J. Chem. Phys. **120**, 5235 (2004).
- [19] E. R. Weeks, J. C. Crocker, and D. A. Weitz, J. Phys.: Cond. Matter **19**, 205131 (2007).
- [20] G. Szamel and E. Flenner, Phys. Rev. Lett. **107**, 105505 (2011).
- [21] E. Flenner and G. Szamel, J. Phys.: Cond. Matter **27**, 194125 (2015).
- [22] T. M. Cover and J. A. Thomas, *Elements of Information Theory* (John Wiley and Sons, 2006).
- [23] R. T. Wicks, S. C. Chapman, and R. O. Dendy, Phys. Rev. E **75**, 051125 (2007).
- [24] J. Wilms, M. Troyer, and F. Verstraete, J. Stat. Mech.: Theor. Exp. p. P10011 (2011).
- [25] J. Wilms, J. Vidal, F. Verstraete, and S. Dusuel, J. Stat. Mech.: Theor. Exp. p. P01023 (2012).
- [26] A. J. Dunleavy, K. Wiesner, R. Yamamoto, and P. Royall, Nat. Comm. **6**, 6089 (2015).
- [27] V. Alba, S. Inglis, and L. Pollet, Phys. Rev. B **93**, 094404 (2016).
- [28] A. B. Belonoshko, N. V. Skorodumova, A. Rosengren, and B. Johansson, Phys. Rev. B **73**, 012201 (2006).
- [29] S. Davis, C. Loyola, F. González, and J. Peralta, Comp. Phys. Comm. **181**, 2126 (2010).

- [30] D. Alfè, C. Cazorla, and M. J. Gillan, *J. Chem. Phys.* **135**, 024102 (2011).
- [31] S. Davis, C. Loyola, and J. Peralta, *Phys. A* **515**, 546 (2019).
- [32] R. W. Balluffi, S. M. Allen, and W. C. Carter, *Kinetics of Materials* (Wiley-Interscience, 2005).
- [33] C. A. L. Bailer-Jones, *Practical Bayesian Inference* (Cambridge University Press, 2017).
- [34] E. M. Pearson, T. Halicioglu, and W. A. Tiller, *Phys. Rev. A* **32**, 3030 (1985).
- [35] J. R. Ray, *Phys. Rev. A* **44**, 4061 (1991).
- [36] S. Davis, *Physical Review E* **84**, 50101 (2011).